Available online at www.sciencedirect.com

SCIENCE DIRECT®

Synthetic Metals 151 (2005) 231–238

SYNTHETIC METALS

www.elsevier.com/locate/synmet

Crystal structure and magnetic properties of an ionic multi-component complex of fullerene $(OMTTF{\cdot}I_3){\cdot}C_{60}$ Comparison with $OMTTF{\cdot}I_3$ salts

Dmitri V. Konarev [a,b,*], Salavat S. Khasanov [a,c], Akihiro Otsuka [a,d],
Gunzi Saito [a,**], Rimma N. Lyubovskaya [b]

[a] *Division of Chemistry, Graduate School of Science, Kyoto University, Sakyo-ku, Kyoto 606-8502, Japan*
[b] *Institute of Problems of Chemical Physics RAS, Chernogolovka, Moscow Region 142432, Russia*
[c] *Institute of Solid State Physics RAS, Chernogolovka, Moscow Region 142432, Russia*
[d] *Research Center for Low Temperature and Materials Sciences, Kyoto University, Sakyo-ku, Kyoto 606-8502, Japan*

Received 8 April 2005; received in revised form 10 May 2005; accepted 16 May 2005
Available online 1 July 2005

Abstract

A new ionic multi-component complex $(OMTTF{\cdot}I_3){\cdot}C_{60}$ comprising neutral C_{60} molecules and $OMTTF^{\bullet +}$ and I_3^- ions has been obtained by the diffusion method. The complex has a layered structure with the alternation of closely packed hexagonal C_{60} layers and the layers composed of $OMTTF^{\bullet +}$ and I_3^- ions arranged in a chequer-like manner. The polycrystalline complex shows a strongly asymmetric EPR signal consisting of four components in the 4–293 K range attributable to $OMTTF^{\bullet +}$. Temperature dependent magnetic susceptibility indicates an antiferromagnetic interaction of spins localized on $OMTTF^{\bullet +}$ with an antiferromagnetic hump near 4.5 K. According to the one-dimensional Heisenberg antiferromagnet model the exchange interaction was estimated to be $J/k_B = -3.3$ K. Two possible pathways contribute to this interaction: through the diamagnetic I_3^- anions and the direct interaction between adjacent $OMTTF^{\bullet +}$. The crystal structures of three phases of the $OMTTF{\cdot}I_3$ salt are also presented.

1. Introduction

Donor–acceptor complexes of fullerenes show intriguing optical [1], conducting and magnetic properties [2–4]. However, fullerenes are relatively weak acceptors ($E^{0/-} = -0.44$ V versus SCE for C_{60} [5]) and form mainly neutral solid complexes with organic donors (D_1): amines [6], aromatic hydrocarbons [7,8], substituted tetrathiafulvalenes [9,10], porphyrins [11,12] and others [10]. We developed a multi-component approach, which allows the preparation of fullerene complexes with radical cations of organic donors such as substituted tetrathiafulvalenes. Previously we developed two synthetic procedures to prepare such complexes. Two phases of $\{(BEDT\text{-}TTF^{\bullet +}){\cdot}(I_3^-)\}{\cdot}C_{60}$ (bis(ethylenedithio)tetrathiafulvalene (BEDT-TTF)) were prepared by the recrystallization of the $BEDT\text{-}TTF{\cdot}I_{3.5}$ salt from a saturated C_{60} benzonitrile/*o*-dichlorobenzene solution [13] and by the diffusion of acetonitrile solution of I_2 into a toluene/*o*-dichlorobenzene solution containing C_{60} and BEDT-TTF [14]. $(BEDT\text{-}TTF{\cdot}I_3){\cdot}C_{60}$ is a layered compound, in which closely packed C_{60} layers alternate with the layers composed of $BEDT\text{-}TTF^{\bullet +}$ and I_3^- ions [14]. To expand a range of multi-component ionic complexes of fullerenes we used another substituted tetrathiafulvalene, namely octamethylenetetrathiafulvalene (OMTTF) containing only four sulfur atoms instead of eight ones in BEDT-TTF. Here we report the synthesis, crystal structure, optical and magnetic properties of $\{(OMTTF^{\bullet +}){\cdot}(I_3^-)\}{\cdot}C_{60}$ (**1**) as well as the crystal structures of three phases of $(OMTTF^{\bullet +}){\cdot}(I_3^-)$

---

[*] Corresponding author. Fax: +7 096 515 54 20.
[**] Corresponding author. Fax: +81 75 754 40 35.
E-mail addresses: konarev@icp.ac.ru (D.V. Konarev), saito@kuchem.kyoto-u.ac.jp (G. Saito).

0379-6779/$ – see front matter © 2005 Elsevier B.V. All rights reserved.
doi:10.1016/j.synthmet.2005.05.003

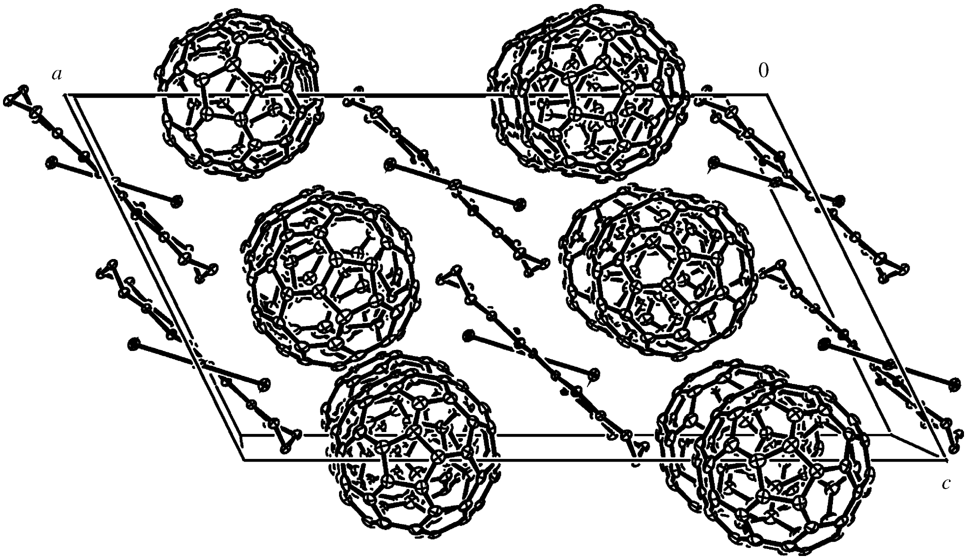

Fig. 1. The view of the crystal structure of **1** along the *b*-axis.

salt (**2–4**). IR-, UV–vis–NIR-, EPR spectra and the data of magnetic susceptibility measurements for **1** are discussed.

2. Results and discussion

The crystals of (OMTTF·I_3)·C_{60} (**1**) were prepared by the diffusion method. OMTTF·I_3 salt is essentially more soluble in acetonitrile than BEDT-TTF·I_3. Because of this, the use of pure acetonitrile in the synthesis provided the formation of a mixture of pure C_{60} crystals and different phases of the OMTTF·I_3 salt. Acetonitrile was mixed with toluene at a 3:1 volume ratio to lower solubility of OMTTF·I_3, and in this case only complex **1** crystallized during diffusion. The diffusion of acetonitrile solution of I_2 into a toluene solution of OMTTF afforded crystals of the OMTTF·I_3 salt, whose three phases (**2–4**) were separated according to the shape under a microscope.

1 is isomorphous to (BEDT-TTF·I_3)·C_{60} [14]. According to single crystal X-ray diffraction data for **1**, C_{60}, OMTTF$^{\bullet+}$ and I_3^- are fully ordered and reside in special positions on two-fold axes (Fig. 1). Densely packed hexagonal C_{60} layers are parallel to the *bc*-plane and alternate with the ionic layers composed of OMTTF$^{\bullet+}$ and I_3^- ions. The distances

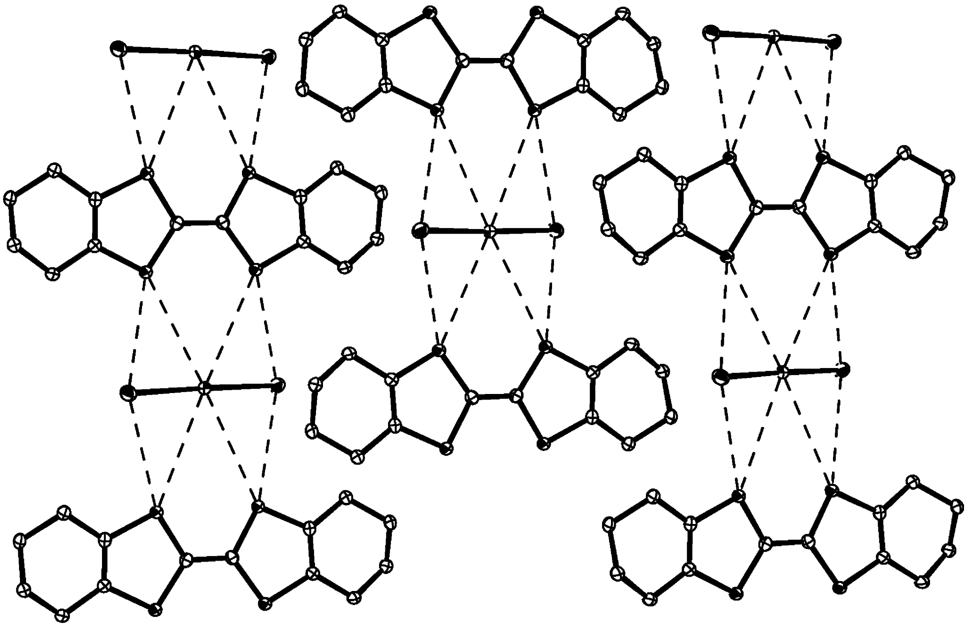

Fig. 2. The projection of the ionic layers in **1** containing OMTTF$^{\bullet+}$ and I_3^- ions on the *bc*-plane. The S···I van der Waals contacts (<4 Å) are shown by dashed lines.

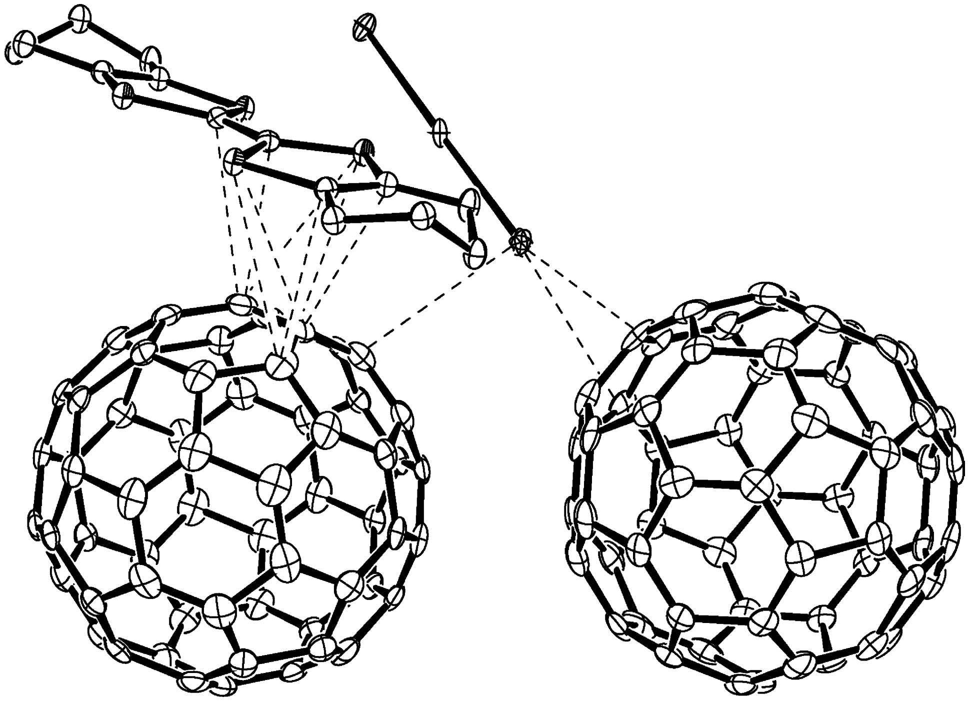

Fig. 3. The shortened van der Waals contacts between OMTTF$^{\bullet +}$ and I_3^- ions and neutral C_{60} molecule in **1** (dashed lines).

between the adjacent C_{60} layers are 14.83 Å. Within the layer each C_{60} molecule has six neighbors with the center-to-center distances equal to 9.94 (four neighbors) and 9.99 Å (two neighbors) and the van der Waals C· · ·C contacts in the 3.12–3.51 Å range. OMTTF$^{\bullet +}$ and I_3^- ions arrange in the ionic layers in a chequer-like manner. The C· · ·C and C· · ·S contacts between the adjacent OMTTF$^{\bullet +}$ are larger than 3.7 Å. Nevertheless, OMTTF$^{\bullet +}$ alternates with I_3^- ions along the *b*-axis and forms van der Waals S· · ·I contacts in the 3.85–3.91 Å range (Fig. 2, dashed lines).

Neutral C_{60} layers, and ionic OMTTF$^{\bullet +}$·I_3^- layers are held together by van der Waals forces (Fig. 3). OMTTF$^{\bullet +}$ forms van der Waals contacts only with two fullerene molecules (the second C_{60} molecule is not depicted in Fig. 3), whereas BEDT-TTF$^{\bullet +}$ forms such contacts with six fullerene molecules in (BEDT-TTF·I_3)·C_{60} [14]. The S and C(OMTTF$^{\bullet +}$)· · ·C(C_{60}) contacts lie in the 3.37–3.78 and 3.20–3.40 Å range, respectively. Linear I_3^- anions extend into the cavities in the C_{60} layer and form van der Waals contacts with two fullerene molecules (the I· · ·C distances are 3.70–3.95 Å) (Fig. 3).

OMTTF$^{\bullet +}$ has an almost planar shape in **1**. However, the formation of short contacts with a spherical fullerene molecule results in some deviations from planarity. The central S_4C_2 fragment is not fully planar and twisted about the central C=C bond. A torsion angle between two planes formed by two S_2C fragments is 171.7°. The six-membered outer rings of OMTTF$^{\bullet +}$ have “twist” conformation, where two carbon atoms of the ethylene group are located on different sides of the C_4S_2C plane. The central C=C bond length in OMTTF$^{\bullet +}$ of 1.398(4) Å is close to that in HMTTF$^{\bullet +}$ in HMTTF·I_3 (1.400(12) and 1.382(16) Å [15]). Thus, the structural data indicate approximately +1 charge on the OMTTF molecule.

It is interesting to compare the crystal structure of **1** with that of a neutral OMTTF·C_{60}·C_6H_6 complex [9]. The latter complex has a layered structure with the alternation of closely packed C_{60} layers and the layers composed of neutral OMTTF and solvent C_6H_6 molecules. However, the OMTTF and C_6H_6 molecules form uniform chains passing along the *a*-axis [9]. The chequered packing motif in **1** is probably more favorable for the electrostatic interaction between OMTTF$^{\bullet +}$ and I_3^- ions. The similarity of the crystal structures of **1** and OMTTF·C_{60}·C_6H_6 is associated with similar nearly planar geometry of OMTTF in neutral and charged forms in the complexes with C_{60}. On the contrary, the crystal structure of ionic (BEDT-TTF·I_3)·C_{60} [14] is completely different from that of neutral (BEDT-TTF)$_2$·C_{60} [16] since BEDT-TTF is planar in a charged form and can essentially bend in a neutral state when forming a complexe with C_{60}. The formation of a multi-component ionic complex of C_{60} with OMTTF$^{\bullet +}$ can be considered as a substitution of a solvent molecule in a neutral complex by oxidant (I_3^-) in solution. Previously, the doping of some solvent-containing C_{60} complexes by iodine vapor also resulted in the substitution of solvent molecules and was accompanied by the formation of ionic multi-component complexes: $\{(D^{\bullet +})\cdot(I_x^-)\}\cdot C_{60}$ (D, tetraphenyldipyranylidene; tetramethylenedithiadimethyltetrathiafulvalene and dibenzotetrathiafulvalene). However, crystalline materials cannot be prepared by doping probably

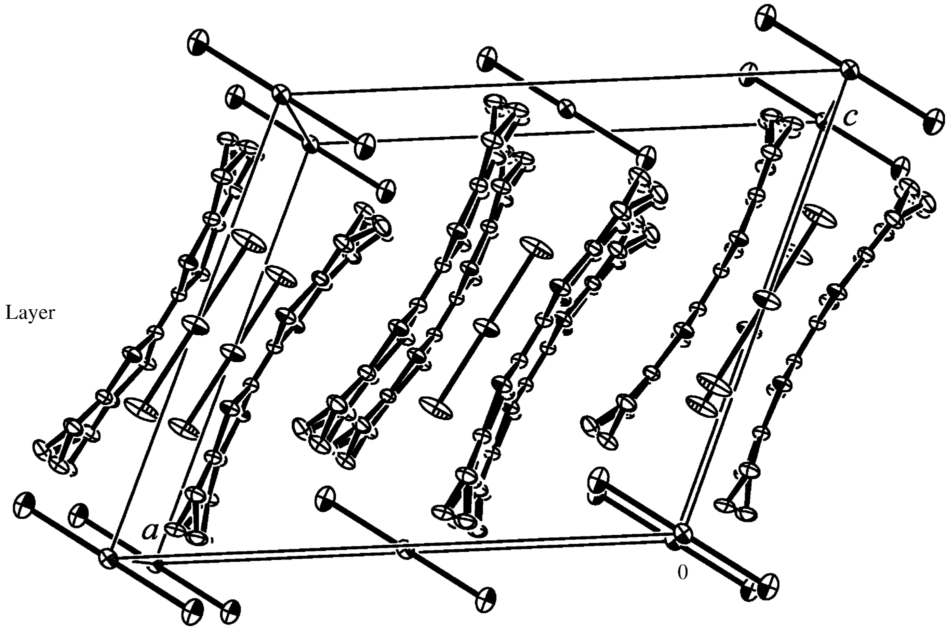

Fig. 4. The view of the crystal structure of **2** along the *b*-axis.

due to a non-uniform distribution of iodine in crystals [17].

We solved crystal structures of three phases of the OMTTF·I_3 salt additionally to that of **1** (Figs. 4 (**2**), 5 (**3**) and 6 (**4**)). Previously the crystal structure of iodine radical cation salt of hexamethylenetetrathiafulvalene, HMTTF·I_3 was studied [15]. However, the crystal structure of the OMTTF·I_3 salt has not been solved yet.

OMTTF$^{\bullet +}$ forms π-dimers in **2** and **3**. The central S_4C_2 fragments of OMTTF$^{\bullet +}$ in such dimers are almost parallel (the corresponding dihedral angles are 0 (**2**) and 2.1° (**3**)) and form van der Waals S· · ·S and C· · ·C contacts of about 3.36 Å in **2**, and 3.31 Å in **3**.

In the crystal structure of **2** the layers parallel to the *ab*-plane can be outlined (Fig. 4, layer). Within these layers π-dimers from OMTTF$^{\bullet +}$ alternate with the linear I_3^-

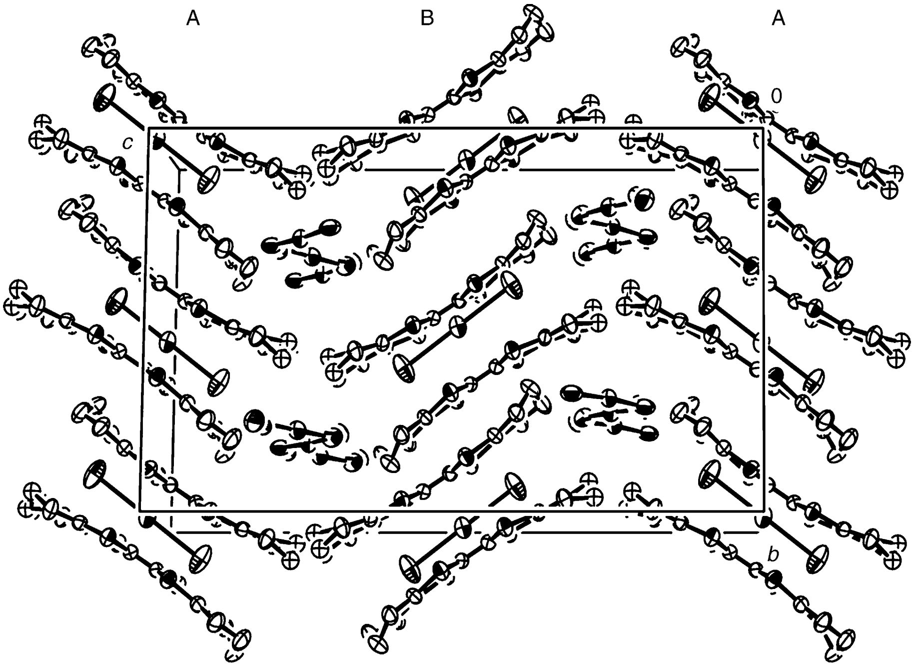

Fig. 5. The view of the crystal structure of **3** along the *a*-axis.

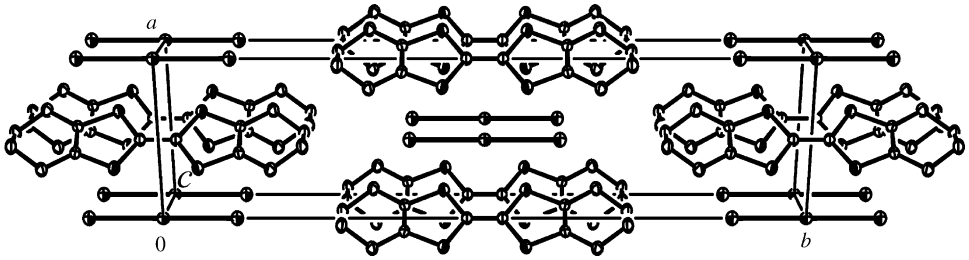

Fig. 6. The view of the crystal structure of **4** along the *c*-axis.

anions in a chequered manner. As this takes place, the I_3^- anions are parallel to the central C=C bond of $OMTTF^{\bullet+}$ and form several S···I contacts of 3.84–3.94 Å length. The other type I_3^- anions positioned between the layers are oriented perpendicular to the central C=C bond of $OMTTF^{\bullet+}$ and form no shortened contacts with them.

Similar ionic layers are also formed in **3** and are arranged parallel to the *ab*-plane. The different orientation of $OMTTF^{\bullet+}$ and I_3^- ions in the adjacent layer relative to the *c*-axis allows layers **A** and **B** to be distinguished (Fig. 5). The I_3^- anions within the layers **A** and **B** arrange parallel to the central C=C bond of $OMTTF^{\bullet+}$ and form S···I contacts of 3.82–4.10 Å length. The I_3^- anions positioned outside the layers form separate zig-zag chains passing along the *a*-axis. These anions form no shortened contacts with $OMTTF^{\bullet+}$.

Geometry of $OMTTF^{\bullet+}$ in **2** and **3** is different from that in **1** since $OMTTF^{\bullet+}$ is slightly bent with a dihedral angle between the central planar S_4C_2 fragment and the planes of outer S_2C_4 fragments of 7.9 and 9.8° for **2** and 7.1 and 9.0° for **3**. The outer six-membered rings of $OMTTF^{\bullet+}$ have "boat" conformation, when both carbon atoms of disordered ethylene groups are located on the same side (above or below) of the C_4S_2C plane. The central C=C length bond in OMTTF is 1.394(2) Å in **2** and 1.387(2) Å in **3** indicating approximately +1 charge on the molecule.

The crystal structure of **4** contains uniform separate stacks of $OMTTF^{\bullet+}$ and I_3^- ions passing along the *c*-axis (Fig. 6). There is no overlapping between the $OMTTF^{\bullet+}$ radical cations (the shortest intermolecular S···S contacts >3.98 Å) and I_3^- ions (the I···I contacts >5.73 Å) in the stacks, whereas multiple van der Waals S···I contacts of 3.91–4.10 Å length are formed between the stacks. $OMTTF^{\bullet+}$ has a planar $C_{12}S_4$ fragment with outer ethylene carbon atoms in "twist" conformation. The central C=C bond length is 1.401(2) Å.

The UV–vis–NIR spectra of $(OMTTF{\cdot}I_3){\cdot}C_{60}$ (**1**), $OMTTF{\cdot}I_3$ (**2**) and neutral $OMTTF{\cdot}C_{60}{\cdot}C_6H_6$ [9] are shown for comparison in Fig. 7a–c. The bands in the UV-range at 38.3 and $29.7 \times 10^3\,cm^{-1}$ in the spectrum of **1** (Fig. 7b) are attributed to C_{60}. Closely positioned bands were also observed for neutral $OMTTF{\cdot}C_{60}{\cdot}C_6H_6$ (37.2 and $29.2 \times 10^3\,cm^{-1}$, Fig. 7c) [9]. $OMTTF^{\bullet+}$ has two characteristic bands in the visible range corresponding to intramolecular transitions. These bands are positoned at 17.0–17.6 and $23.4–24.5 \times 10^3\,cm^{-1}$ (bands D and E, respectively) in different salts containing +1 charged OMTTF: OMTTF·Br, $(OMTTF)_2{\cdot}[Ni(dto)_2]$ (dto: dithiooxalate) [18]. Similar bands are also revealed in the spectrum of **2** (16.0 and $22 \times 10^3\,cm^{-1}$, Fig. 7a) and **1** (16 and $23 \times 10^3\,cm^{-1}$, Fig. 7b). Broad absorption with the maximum near $11 \times 10^3\,cm^{-1}$ in the spectrum of **2** (Fig. 7a, CT_1) most probably originates from intermolecular transitions between $OMTTF^{\bullet+}$ in the π-dimers. Other OMTTF salts containing such dimers manifest this band at $11.5 \times 10^3\,cm^{-1}$ [18]. Since the $OMTTF^{\bullet+}$ radical cations are isolated from each other in **1**, the CT_1 band is absent in the spectrum (Fig. 7b). The spectrum of neutral $OMTTF{\cdot}C_{60}{\cdot}C_6H_6$ also contains an additional low-energy band at $10.9 \times 10^3\,cm^{-1}$ (Fig. 7c, CT_2) attributed to CT from neutral OMTTF to C_{60} molecules [9] and a band at $21.2 \times 10^3\,cm^{-1}$ (Fig. 7c, CT_3), which can be attributed to intermolecular CT between neighboring C_{60} molecules [19]. The latter band is characteristic of complexes with closely packed C_{60} molecules [10,20] and can also contribute to the absorption band at $23 \times 10^3\,cm^{-1}$ in the spectrum of **1** (these transitions are possible both in $OMTTF{\cdot}C_{60}{\cdot}C_6H_6$ and **1** containing closely packed C_{60} layers).

The IR-spectrum of **1** indicates the presence of neutral C_{60} (526, 576, 1182 and 1427 cm^{-1}) and the $OMTTF^{\bullet+}$ radical cation (460, 813, 988, 1074, 1171, 1236, 1262, 1326, 1348, 1442 and 1537 cm^{-1}). The $OMTTF{\cdot}I_3$ salt (**2**) has close posi-

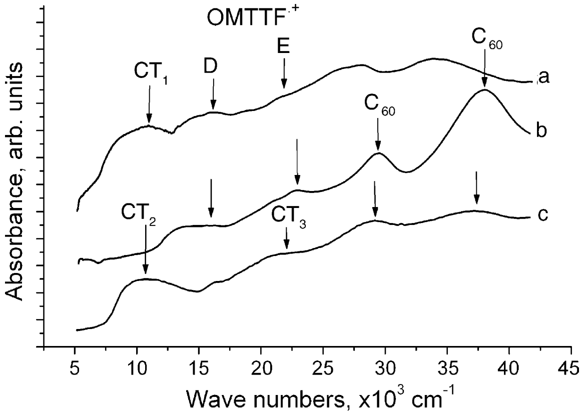

Fig. 7. UV–vis–NIR optical absorption spectra of $OMTTF{\cdot}I_3$ (**2**) (a); $(OMTTF{\cdot}I_3){\cdot}C_{60}$ (**1**) (b) and $OMTTF{\cdot}C_{60}{\cdot}C_6H_6$ [9] (c) in the $5–42 \times 10^3\,cm^{-1}$ range in KBr pellets.

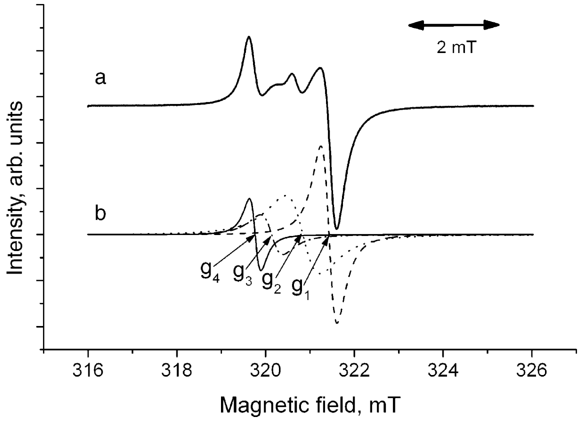

Fig. 8. EPR spectrum of polycrystalline OMTTF·I_3·C_{60} (**1**) at 250 K (a) and below is the simulation of the signal by four Lorentzian lines (b).

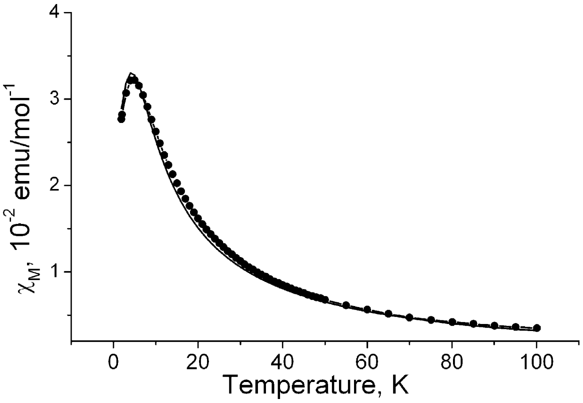

Fig. 9. Temperature dependence of molar magnetic susceptibility of 1 in the 1.9–100 K range in the applied field 100 mT. The solid line denotes theoretical fitting according to the one-dimensional Heisenberg antiferromagnet model [21].

tions of the absorption bands in the IR-spectrum (461, 811, 992, 1074, 1236, 1260, 1331, 1344, 1418, 1457, 1540 and 1554 cm^{-1}).

Polycrystalline **1** shows a strongly asymmetric EPR signal, which can be simulated by four Lorentzian lines with g-factors: $g_1 = 2.0067$ (the line halfwidth $\Delta H = 0.34$ mT), $g_2 = 2.0095$ ($\Delta H = 0.63$ mT), $g_3 = 2.0137$ ($\Delta H = 0.71$ mT), and $g_4 = 2.0172$ ($\Delta H = 0.34$ mT) at 250 K (Fig. 8). This signal can be attributed to OMTTF$^{\bullet +}$. Related polycrystalline (BEDT-TTF·I_3)·C_{60} has a symmetric single line with $g = 2.0074$ ($\Delta H = 2.3$ mT) at room temperature and $g = 2.0074$ ($\Delta H = 2.0$ mT) at 77 K [14]. Decreasing temperature does not change the shape of the signal of **1** and the line halfwidths of the Lorentzian components. The spectrum of **1** at 5 K can be simulated by four Lorentzian lines with $g_1 = 2.0072$ ($\Delta H = 0.36$ mT), $g_2 = 2.0109$ ($\Delta H = 0.78$ mT), $g_3 = 2.0153$ ($\Delta H = 0.50$ mT) and $g_4 = 2.0177$ ($\Delta H = 0.27$ mT).

The temperature dependence of magnetic susceptibility of **1** shows the Curie–Weiss behavior with the Weiss constant of $\Theta = -2.7$ K (above 20 K) indicating a weak antiferromagnetic interaction of spins. Fig. 9 represents a portion of the T dependence of susceptibility for **1** in the 100 - 1.9 K range. Susceptibility attains the maximum at 4.5 K and then decreases with temperature. This hump can be attributed to an antiferromagnetic interaction of spins localized on OMTTF$^{\bullet +}$. The fitting of the data by the one-dimensional Heisenberg antiferromagnet model in the 100–1.9 K range allows the estimation of the exchange interaction between OMTTF$^{\bullet +}$ spins with $J/k_B = -3.3$ K (Fig. 9). The fitting of the data by the two-dimensional Heisenberg antiferromagnet model is in a poorer agreement with experiment.

To estimate possible pathways for the antiferromagnetic exchange interaction between OMTTF$^{\bullet +}$ spins we calculated intermolecular overlap integrals based on an extended Hückel method within the ionic layers formed by OMTTF$^{\bullet +}$ and I_3^- and arranged parallel to the bc-plane (Fig. 10). An obvious interaction is observed between OMTTF$^{\bullet +}$ and I_3^- in the transverse directions at the same height along the b-axis (p1 and p2 in Fig. 10). The other weak, but non-negligible interactions were obtained among adjacent OMTTF$^{\bullet +}$ radical cations in the diagonal direction (q1 and q2 in Fig. 10). Thus, there are two possible ways for a one-dimensional antiferromagnetic interaction between OMTTF$^{\bullet +}$ spins, though it is not clear what interaction dominates: either through the diamagnetic I_3^- anions or directly between each other.

Complex **1** is a semiconductor with room-temperature conductivity $\sigma = 10^{-5}$ S cm^{-1}. Such conductivity is characteristic of simple salts with full +1 charge on the molecule [15,22,23] and is close to that of (BEDT-TTF·I_3)·C_{60} [14].

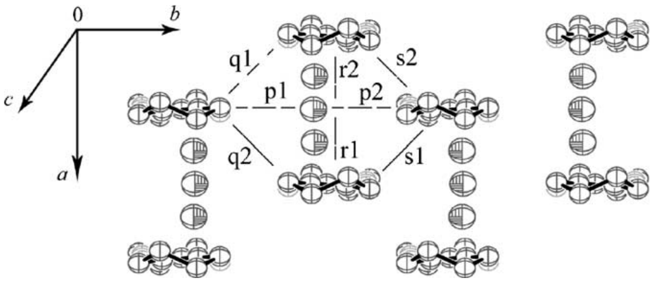

p1	-1.74×10^{-3}
p2	-1.00×10^{-3}
q1	0.57×10^{-3}
q2	0.56×10^{-3}
r1	-0.16×10^{-3}
r2	-0.10×10^{-3}
s1	0.92×10^{-4}
s2	0.89×10^{-4}

Fig. 10. Overlap integrals between OMTTF$^{\bullet +}$ and I_3^- ions within the layer in **1**. Projection is approximately parallel to the molecular long axis of OMTTF$^{\bullet +}$.

3. Conclusion

A new multi-component C_{60} complex containing $OMTTF^{\bullet+}$ radical cations and the I_3^- anions was obtained by the diffusion method. **1** is specified by a layered structure with closely packed hexagonal neutral C_{60} layers and ionic $OMTTF^{\bullet+}$ and I_3^- layers. Two types of layers are held together by van der Waals forces. Electrostatic interaction plays an important role within the ionic layers and provides a chequered arrangement of the ions similar to that for ionic layers in simple fullerene free $OMTTF{\cdot}I_3$ salts (**2** and **3**). Complex **1** is isomorphous to previously characterized $(BEDT\text{-}TTF{\cdot}I_3){\cdot}C_{60}$. However, a smaller number of sulfur atoms in OMTTF results in the essential decrease in a number of van der Waals contacts between C_{60} and $OMTTF^{\bullet+}$. The crystal structure of **1** is similar to that of neutral $OMTTF{\cdot}C_{60}{\cdot}C_6H_6$. The positions of solvent C_6H_6 molecules in $OMTTF{\cdot}C_{60}{\cdot}C_6H_6$ and the I_3^- anions in **1** are close, and the synthesis of an ionic multi-component complex can be considered as a substitution of solvent molecules by oxidant (I_2) in the solution synthesis. Previously such a substitution was realized by a doping of neutral complexes containing solvent by iodine vapor. However, crystalline materials cannot be prepared by this method. According to EPR and magnetic susceptibility measurements spins are localized in **1** on $OMTTF^{\bullet+}$ and show weak antiferromagnetic coupling (the Weiss constant is −2.7 K) that results in the decrease of magnetic susceptibility below 4.5 K. Two possible pathways contribute to the one-dimensional exchange interaction: through the diamagnetic I_3^- anions and the direct interaction between adjacent $OMTTF^{\bullet+}$. Both pathways provide a rather large distance between spins localized on $OMTTF^{\bullet+}$ and as a result, the observed antiferromagnetic interaction is relatively weak with the exchange interaction $J/k_B = -3.3$ K.

4. Experimental

4.1. Materials

C_{60} of 99.98% purity was used from MTR Ltd. Toluene (C_6H_5Me) was distilled over Na/benzophenone in the argon atmosphere. Acetonitrile (CH_3CN) was distilled over CaH_2, P_2O_5 and K_2CO_3 under argon.

4.2. General

FT IR spectra were measured in KBr pellets with a Perkin-Elmer 1000 Series spectrometer (400–7800 cm^{-1}). UV–vis–NIR spectra were measured on a Shimadzu-3100 spectrometer in the 220–1600 nm range. EPR spectra were recorded down to 4 K with a JEOL JES-TE 200 X-band ESR spectrometer equipped with a JEOL ES-CT470 cryostat. A Quantum Design MPMS-XL SQUID magnetometer was used to measure static susceptibilities between 300 and 1.9 K. A sample holder contribution and core temperature independent diamagnetic susceptibility (χ_0) were subtracted from the experimental values. The values of C, Θ and χ_0 were calculated from the high-temperature range using the appropriate formula: $\chi_M = C/(T - \Theta) + \chi_0$. The molecular overlap integrals (S) in **1** were obtained from the structure of ionic layer in **1** at 120 K by applying the simple extended Hückel method [24]. The extended Hückel parameters for iodine atom were taken from Summerville and Hoffmann [25], while those for carbon, hydrogen and sulfur atoms were taken from Mori et al. [24].

4.3. Synthesis

The crystals of $(OMTTF{\cdot}I_3){\cdot}C_{60}$ (**1**) were obtained by a slow diffusion of acetonitrile/toluene (3/1) solution (20 mL) of I_2 (21 mg, 0.083 mmol) into the toluene solution (20 mL), containing C_{60} (20 mg, 0.027 mmol) and OMTTF (17 mg, 0.054 mmol) at a 1:2 molar ratio. Diffusion was carried out in a glass tube of 1.5 cm diameter and 40 mL volume with a ground glass plug. After 1 month the crystals of **1** formed on the wall of the tube. The solvent was decanted and the crystals were washed with acetonitrile yielding black elongated plates up to 2 mm × 0.6 mm × 0.1 mm size with 70% yield. The composition of **1** was determined from the elemental analysis and was justified by the X-ray diffraction. Found, C = 62.28%; H = 1.78%; S = 9.24%; I = 26.44%; Calc. C = 62.90%; H = 1.13%; S = 9.04%; I = 26.93%.

The crystals of $OMTTF{\cdot}I_3$ were obtained by the diffusion method. The solution of I_2 (36.5 mg, 0.096 mmol) in acetonitrile diffuses into the toluene solution of OMTTF (30 mg, 0.144 mmol). After 1 month the crystals formed on the wall of the tube. The solvent was decanted and the crystals were washed with hexane yielding black parallelograms (**2**) up to 1 mm × 0.3 mm × 0.3 mm size with 40% yield. The second and third phases were obtained in the same synthesis as elongated parallelepipeds with 10% yield (**3**) and black prisms with 30% yield (**4**). The crystals of **2–4** were separated under microscope according to the shape. The composition of the complexes was determined from the X-ray diffraction analysis on a single crystal.

4.4. X-ray crystallography

Crystal data for **1**: $C_{74}H_{16}I_3S_4$, $M_r = 1413.81$, black, crystal size $(0.6 \times 0.3 \times 0.1)\ mm^{-3}$, monoclinic, C2/c, $a = 29.662(3)$, $b = 9.988(1)$, $c = 17.189(1)$ Å, $\beta = 116.190(3)°$ $V = 4569.7(7)$ Å^3, $D_c = 2.06\ g\ cm^{-1}$, $Z = 4$, $T = 120(2)$ K, absorption coefficient 2.29 mm^{-1}, $F(0\,0\,0) = 2732$. The least-square refinement on F^2 was done to $R_1 = 0.0338$ for 3704 observed reflections with $[F^2 > 2\sigma(F^2)]$, $wR_2 = 0.089$, data/restrains/parameters 4088/827/368, final GoF = 1.024, CCDC reference number is 259895.

Crystal data for **2**: $C_{14}H_{16}I_3S_4$, $M_r = 693.21$, black, crystal size $(0.5 \times 0.12 \times 0.06)\ mm^{-3}$, monoclinic, C2/m, $a = 16.670(1)$, $b = 9.180(1)$, $c = 14.426(1)$ Å, $\beta = 112.411(3)$ Å, $V = 2041.3(3)$ Å^3, $D_c = 2.26\ g\ cm^{-1}$, $Z = 4$, $T = 293(2)$ K, absorption coefficient 5.00 mm^{-1}, $F(0\,0\,0) = 1292$. The least-square refinement on F^2 was done to $R_1 = 0.035$ for 1871 observed reflections with $[F^2 > 2\sigma(F^2)]$, $wR_2 = 0.09$, data/restrains/parameters 2164/0/135, final GoF = 1.113, CCDC reference number is 259893.

Crystal data for **3**: $C_{14}H_{16}I_3S_4$, $M_r = 693.21$, black, crystal size $(0.4 \times 0.12 \times 0.05)$ mm^{-3}, orthorombic, $C222_1$, $a = 9.581(4)$, $b = 15.824(6)$, $c = 26.594(4)$ Å, $V = 4031.9(6)$ Å^3, $D_c = 2.28$ g cm^{-1}, $Z = 8$, $T = 293(2)$ K, absorption coefficient 5.06 mm^{-1}, $F(0\,0\,0) = 2584$. The least-square refinement on F^2 was done to $R_1 = 0.0335$ for 2020 observed reflections with $[F^2 > 2\sigma(F^2)]$, $wR_2 = 0.086$, data/restrains/parameters 2176/12/215, final GoF = 1.078, CCDC reference number is 259894.

Crystal data for **4**: $C_{14}H_{16}I_3S_4$, $M_r = 693.21$, black, crystal size $(0.4 \times 0.18 \times 0.14)$ mm^{-3}, monoclinic, C2/m, $a = 7.7696(8)$, $b = 25.2965(15)$, $c = 5.7335(6)$ Å, $\beta = 118.871(7)^\circ$, $V = 986.8(2)$ Å^3, $D_c = 2.33$ g cm^{-1}, $Z = 2$, $T = 293(2)$ K, absorption coefficient 5.17 mm^{-1}, $F(0\,0\,0) = 646$. The least-square refinement on F^2 was done to $R_1 = 0.0166$ for 723 observed reflections with $[F^2 > 2\sigma(F^2)]$, $wR_2 = 0.0391$, data/restrains/parameters 848/0/52, final GoF = 1.078, CCDC reference number is 259892.

The intensity data for the structural analysis were collected for **1**–**3** on a MAC Science DIP-2020K oscillator type X-ray imaging plate diffractometer and for **4** on a CAD-4F 4-circle diffractometer with graphite monochromated Mo Kα radiation. Raw data reduction to F^2 was carried out using the DENZO program [26] for **1**–**3** and XCAD4 program [27] for **4**. The structures were solved by a direct method and refined by the full-matrix least-squares method against F^2 using SHELX-97 [28].

Acknowledgements

The work was partly supported by a Grant-in-Aid Scientific Research from the Ministry of Education, Culture, Sports, Science and Technology, Japan (152005019, 21st Century COE, and Elements Science 12CE2005) and the RFBR grant N 03-03-32699a.

References

[1] D.M. Guldi, Chem. Soc. Rev. 31 (2002) 22.
[2] M.J. Rosseinsky, J. Mater. Chem. 5 (1995) 1497.
[3] B. Gotschy, Fullerene Sci. Technol. 4 (1996) 677.
[4] D.V. Konarev, R.N. Lyubovskaya, Russ. Chem. Rev. 68 (1999) 19.
[5] D. Dubois, K.M. Kadish, S. Flanagan, R.E. Haufler, L.P.F. Chibante, L.J. Wilson, J. Am. Chem. Soc. 113 (1991) 4363.
[6] D.V. Konarev, A.Yu. Kovalevsky, A.L. Litvinov, N.V. Drichko, B.P. Tarasov, P. Coppens, R.N. Lyubovskaya, J. Solid State Chem. 168 (2002) 474.
[7] D.V. Konarev, Yu.V. Zubavichus, E.F. Valeev, Yu.L. Slovokhotov, Yu.M. Shul‘ga, R.N. Lyubovskaya, Synth. Met. 103 (1999) 2364.
[8] A.L. Litvinov, D.V. Konarev, A.Yu. Kovalevsky, I.S. Neretin, Yu.L. Slovokhotov, P. Coppens, R.N. Lyubovskaya, Cryst. Eng. Commun. 4 (2002) 618.
[9] G. Saito, T. Teramoto, A. Otsuka, Y. Sugita, T. Ban, M. Kusunoki, K. Sakaguchi, Synth. Met. 64 (1994) 359.
[10] D.V. Konarev, R.N. Lyubovskaya, N.V. Drichko, E.I. Yudanova, Yu.M. Shul‘ga, A.L. Litvinov, V.N. Semkin, B.P. Tarasov, J. Mater. Chem. (2000) 803.
[11] M.M. Olmstead, D.A. Costa, K. Maitra, B.C. Noll, S.L. Phillips, P.M. Van Calcar, A.L. Balch, J. Am. Chem. Soc. 121 (1999) 7090.
[12] D.V. Konarev, I.S. Neretin, Yu.L. Slovokhotov, E.I. Yudanova, N.V. Drichko, Yu.M. Shul‘ga, B.P. Tarasov, L.L. Gumanov, A.S. Batsanov, J.A.K. Howard, R.N. Lyubovskaya, Chem. Eur. J. 7 (2001) 2605.
[13] D.V. Konarev, N.V. Drichko, R.N. Lyubovskaya, E.I. Yudanova, Yu.M. Shul‘ga, Y.V. Zubavichus, V.N. Semkin, Russ. Chem. Bull. 48 (1999) 1946.
[14] D.V. Konarev, A.Yu. Kovalevsky, P. Coppens, R.N. Lyubovskaya, Chem. Commun. (2000) 2357.
[15] K. Honda, M. Goto, M. Kurahashi, H. Anzai, M. Tokumoto, H. Bando, T. Ishiguro, Bull. Chem. Soc. Jpn. 60 (1987) 782.
[16] T. Izuoka, T. Tachikawa, Y. Sugawara, M. Suzuki, Y. Konno, H. Saito, H. Shinohara, J. Chem. Soc., Chem. Commum. (1992) 1472.
[17] R.N. Lyubovskaya, D.V. Konarev, E.I. Yudanova, O.S. Roschupkina, Yu.M. Shul‘ga, V.N. Semkin, A. Graja, Synth. Met. 84 (1997) 741.
[18] G. Saito, H. Izukashi, M. Shibata, K. Yoshida, L.A. Kushch, T. Kondo, H. Yamochi, O.O. Drozdova, K. Matsumoto, M. Kusunoki, K. Sakaguchi, N. Kojima, E.B. Yagubskii, J. Mater. Chem. 10 (2000) 893.
[19] M. Ichida, A. Nakamura, H. Shinohara, Y. Saitoh, Chem. Phys. Lett. 289 (1998) 579.
[20] D.V. Konarev, N.V. Drichko, R.N. Lyubovskaya, Yu.M. Shul‘ga, A.L. Litvinov, V.N. Semkin, Yu.A. Dubitsky, A. Zaopo, J. Mol. Struct. 526 (2000) 25.
[21] J.C. Bonner, M.E. Fisher, Phys. Rev. 135 (1964) A640.
[22] R.P. Shibaeva, R.M. Lobkovskaya, E.B. Yagubskii, E.E. Laukina, Sov. Phys. Crystallogr. (Engl. Transl.) 32 (1987) 530.
[23] P. Wang, T. Inabe, C. Nakano, Y. Maruyama, H. Inokuchi, N. Iwasawa, G. Saito, Bull. Chem. Soc. Jpn. 62 (1989) 2252.
[24] T. Mori, A. Kobayashi, Y. Sasaki, H. Kobayashi, G. Saito, H. Inokuchi, Bull. Chem. Soc. Jpn. 57 (1984) 627.
[25] R.H. Summerville, R. Hoffmann, J. Am. Chem. Soc. 98 (1976) 7240.
[26] Z. Otwinowski, W. Minor, in: C.W. Carter, R.M. Sweet (Eds.), Processing of X-ray Diffraction Data Collection in Oscillation Mode, Methods in Enzymology, Academic press, 1997, p. 276.
[27] Harms and Wocaldo, 1995.
[28] G.M. Sheldrick, SHELX97, University of Göttingen, Germany, 1997.